Physica C 201 (1992) 279–288
North-Holland

PHYSICA C

Effect of silver additions on sintered $Bi_2Sr_2CaCu_2O_8$

T.E. Jones, W.C. McGinnis, E.W. Jacobs, R.D. Boss, P.M. Thibado [1], J.S. Briggs and W.E. Glad
Naval Command, Control and Ocean Surveillance Center, RDT&E Division, Materials Research Branch, Code 573, San Diego, CA 92152-5000, USA

Received 8 October 1990
Revised manuscript received 31 July 1992

Up to 30 weight-percent silver has been added, in the form of silver peroxide, prior to the final sintering step in the preparation of the high-T_c superconductor $Bi_2Sr_2CaCu_2O_8$. The sintered samples were characterized by optical microscopy and image analysis, energy-dispersive X-ray analysis, and X-ray diffraction. Intergranular and intragranular critical current densities were measured by transport and magnetization techniques, respectively. Under the sintering conditions used, there is no evidence of silver inclusion in the lattice, nor of any effect on the stoichiometry due to the silver additions. The silver does have a large effect, though, on the sample morphology, and, therefore, on the intergranular critical current density. However, only a modest variation of the intragranular critical current density is observed with added silver.

1. Introduction

The greatest challenge in bringing high-temperature superconductivity into the world of large-scale systems is the attainment of sufficiently high critical current densities. The polycrystalline, ceramic nature of these materials has proved to be a major impediment toward this goal. Our interest in the properties of $Bi_2Sr_2CaCu_2O_8$ with silver additions stems from related work reported on $YBa_2Ca_3O_7$ [1–5]. Silver has proved to be one of the most innocuous or non-poisonous elements for $YBa_2Ca_3O_7$, and there were early reports of large increases (up to 100 times) in the critical current density, J_c, of $YBa_2Ca_3O_7$ with silver additions [1,2]. However, such large increases were observed only on samples that were poorly sintered and consequently had a very low initial J_c. The effect of silver additions on well-sintered samples of $YBa_2Ca_3O_7$ were variously reported as yielding only modest increases [3], having no demonstrable effect [4], or resulting in a monotonic decrease in J_c [5].

Silver has also been shown to be non-poisonous to $Bi_2Sr_2CaCu_2O_8$ and $Bi_2Sr_2Ca_2Cu_3O_{10}$, with the possible exception of samples made with lead [6,7]. The relatively low melting temperature, stability, and tendency toward oriented grain growth of $Bi_2Sr_2CaCu_2O_8$ has led to considerable work in drawing wires of these materials, especially inside silver sheaths [8]. The work reported here was motivated by our early observation that upon adding silver to $Bi_2Sr_2CaCu_2O_8$, both the intergranular and intragranular critical current densities increased with up to a few weight-percent (wt.%) silver [9], and then appeared to decrease for higher concentrations.

This study is a significant extension of previously published work [10], in which only small concentrations of silver, up to 5 wt.%, were added to both $Bi_2Sr_2CaCu_2O_8$ and $Bi_2Sr_2Ca_2Cu_3O_{10}$. The samples used in that work had been sintered with silver for only one hour. No signs of reaction of the silver with the ceramic were observed under those conditions, and there were no discernable changes in the lattice spacings with the addition of silver. The previous work documented the effect of silver on the relative phase composition between $Bi_2Sr_2CaCu_2O_8$ and $Bi_2Sr_2Ca_2Cu_3O_{10}$. It was shown that there is a partial reversibility in the phase composition between $Bi_2Sr_2CaCu_2O_8$, and $Bi_2Sr_2CaCu_3O_{10}$ with the addition of silver. The presence of silver can foster the

[1] Present address: University of Pennsylvania, Department of Physics, 209 S. 33rd Street, Philadelphia, PA 19104-6396, USA.

preferred growth of either phase, depending on the sintering conditions.

The present study extends the previous work in several ways. (1) concentrations of silver up to 30 wt.% are used, (2) the sintering times are as long as 20 h with the silver present, (3) measurements of both transport and magnetization critical current densities are reported for samples with silver concentrations up to 15 wt.%, and (4) extensive microscopic analyses have been performed on samples with silver concentrations up to 30 wt.%. Microscopic image analysis is used to determine how silver is dispersed in the sample, and how silver affects the growth, size, and orientation of $Bi_2Sr_2CaCu_2O_8$ grains. Microscopic chemical analysis of the samples is performed to see if any silver is going into the lattice, and if cation chemistry is affected by the silver.

2. Sample preparation

All chemicals were obtained from Aesar and used as received. The minimum purities were as follows: Bi_2O_3, 99.9998%; $CaCO_3$, 99.9995%; CuO, 99.999%; $SrCO_3$, 99.999%; and Ag_2O_2, 99.9%. Quantities of Bi_2O_3, $SrCO_3$, $CaCO_3$ and CuO, appropriate to achieve the nominal cation ratios for $Bi_2Sr_2CaCu_2O_8$, were well mixed and finely ground. The mixture was calcined at 800°C for a total of 48 h in air in three steps with intermediate grindings. Pellets were then pressed and sintered *without silver* at 848°C for 40 h air. This procedure yields samples that are phase pure with respect to the other known superconducting phases, $Bi_2Sr_2CuO_6$ and $Bi_2Sr_2CaCu_3O_{10}$, as determined by X-ray diffraction. The samples are all metallic, with few discernible impurities, and have superconducting transitions near 80 K.

For the silver additions, a master batch was made by regrinding a set of samples which had been fully sintered as pellets as described above. An appropriate amount of silver peroxide, Ag_2O_2, was added to the reground powder to yield the highest concentration desired. For this study, the maximum concentration prepared was usually 15 or 30 wt.% silver. The master batch of $Bi_2Sr_2CaCu_2O_8$ with silver was then diluted with an appropriate amount of pure $Bi_2Sr_2CaCu_2O_8$ to yield the desired concentration. The diluted powders were well mixed, finely ground, pressed into pellets at a pressure of 280 MPa, and then sintered at 848°C for 20 h in air. It should be noted that the concentration of silver was computed as a fraction of the total weight; that is, $C=100\times W_{Ag}/(W_{Ag}+W_c)$, where C is the quoted concentration in weight-percent silver, W_{Ag} is the weight of silver in the sample, and W_c is the weight of ceramic exclusive of the silver.

3. Results and discussion

A series of optical micrographs were taken of the samples. For these photographs, the samples were set in epoxy, and polished with a series of ever-finer polishing compounds until a satisfactory image resolution was obtained. The photographs were taken with a Neoflot Metallograph Model 21, an optical microscope specifically designed to examine and photograph polished samples such as those prepared for this study. Figure 1 shows a low resolution photograph in cross-section of a 30 wt.% sample. This photograph covers a rather large area of approximately 6300 μm^2 and shows the generally uniform distribution of silver aggregates (the light reflective clusters that appear white) in the sample. Note, however, that there are rather large grains of $Bi_2Sr_2CaCu_2O_8$, or clusters of grains, where there is no visible silver.

Figure 2 is a high resolution photograph of two samples in cross-section. Part (a) shows a control

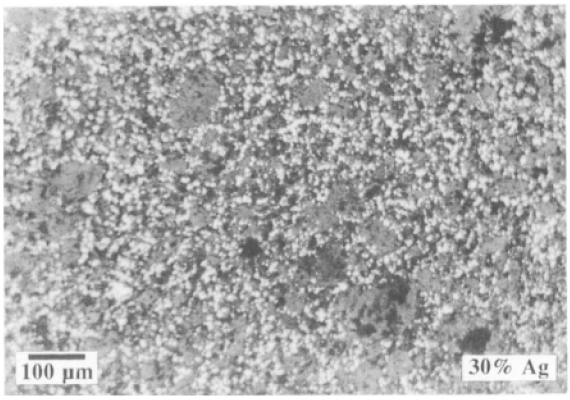

Fig. 1. Photograph in cross-section of a polished sample of $Bi_2Sr_2CaCu_2O_8$ with 30 wt.% silver.

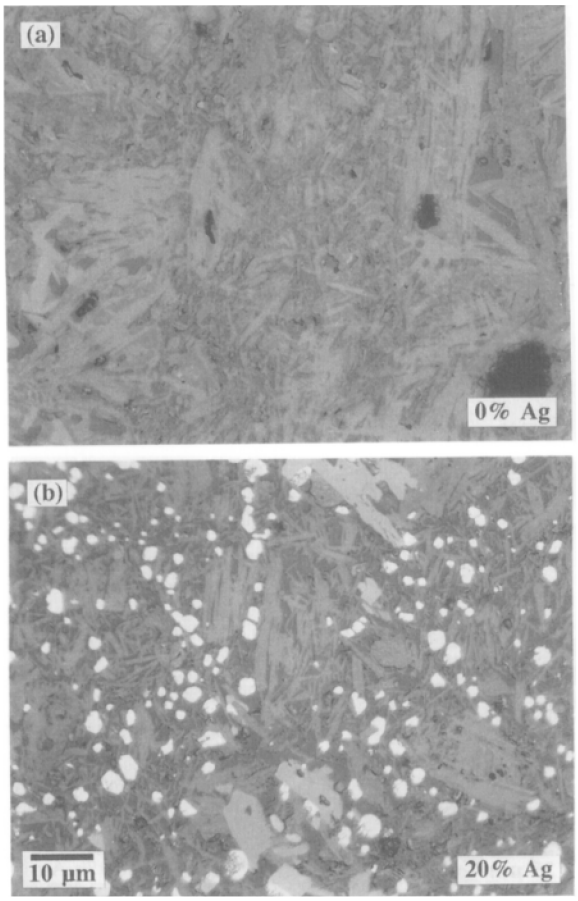

Fig. 2. Photographs in cross-section of polished samples of $Bi_2Sr_2CaCu_2O_8$ with (a) 0 wt.% and (b) 20 wt.% silver. The 10 μm bar applies to both photographs.

sample (0 wt.% silver), and part (b) a sample with 20 wt.% silver. The photographs cover an area of approximately 800 μm^2. In addition to the aggregation of silver that is apparent in part (b), one can also discern a more fragmented grain structure in the highly silver-added sample. This illustrates how the silver aggregates can interfere with the growth of $Bi_2Sr_2CaCu_2O_8$ grains. As was also seen in fig. 1, the visible silver aggregates are not in the $Bi_2Sr_2CaCu_2O_8$ grains themselves, but rather the silver forms clusters that appear to be separate entities in between and adjacent to grains of $Bi_2Sr_2CaCu_2O_8$.

In addition to the optical micrographs taken, these polished samples were also analyzed with a computerized image analyzer system, a Cambridge Instruments Quantimet 970. This instrument allows components of a photograph with high contrast regions, such as the reflective silver clusters in the photographs of figs. 1 and 2, to be analyzed quantitatively for number, size, spacing, separation, etc. Figure 3 shows a set of photographs of intermediate magnification, each covering an area of approximately 1500 μm^2. These photographs were part of a larger set used for the computerized image analysis. Note that, although very little silver aggregation is observable in the 2.5 wt.% sample, all of the silver-added samples contain the nominal amounts of added silver. This was verified by elemental analyses using both inductively coupled plasma (ICP) spectroscopy and coated-wire (Ag/AgCl) ion-selective potentiometry. Thus, we conclude that in samples with 2.5 wt.% silver, either the silver does not aggregate appreciably, or most of the silver clusters are too small to be seen on this scale.

The quantitative results of the computerized image analysis have been summarized in two tables. Table 1 shows, for a set of samples ranging from 5 to 30 wt.% silver, the weight-percent of silver added (column 1), the volume-percent of silver calculated using the known densities of silver and $Bi_2Sr_2CaCu_2O_8$ (column 2), the measured volume-percent of silver as determined by the instrument (column 3), and finally that fraction of the known silver content actually seen (column 4). Note that on the order of 70–80 % of the total silver in the sample is visually observed with the microscope. In other words, most of the silver aggregates as the clusters seen in the photographs of figs. 1–3, and very little silver can be present elsewhere. Recall, with reference to fig. 3, that the 2.5 wt.% sample showed very little silver aggregation. Somewhere in the range of silver concentrations between 2.5 and 5.0 wt.%, the silver forms into visible aggregates. The silver that cannot be accounted for visually must be either in clusters too small to see at the magnification levels used, or incorporated into the $Bi_2Sr_2CaCu_2O_8$ crystal structure. Microscopic elemental analysis and X-ray diffraction measurements have been performed to address this point, and will be discussed below.

In addition to yielding the volume-percent silver shown in table 1, the image analyzer also gives the mean density of silver clusters as well as their mean

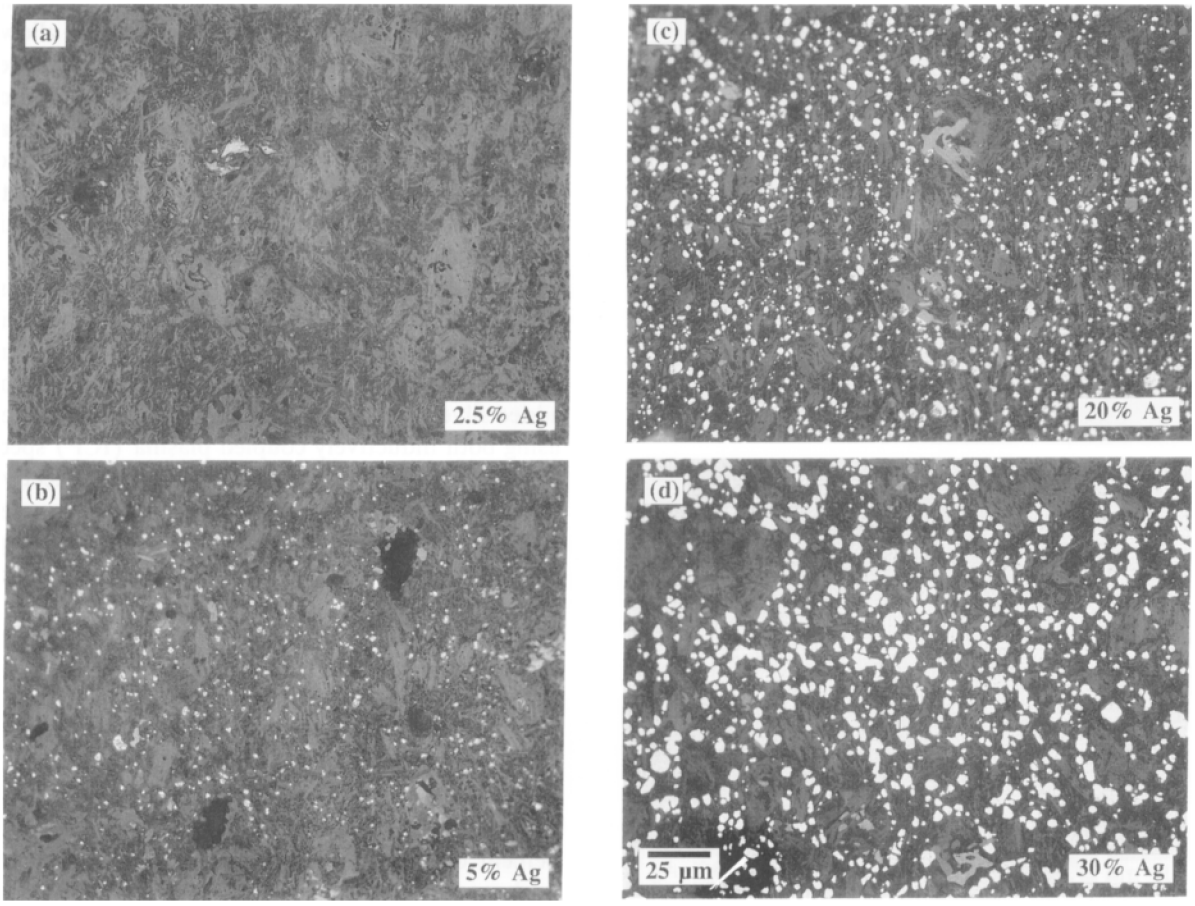

Fig. 3. Photographs of four samples of $Bi_2Sr_2CaCu_2O_8$ with (a) 2.5 wt.%, (b) 5.0 wt.%, (c) 20 wt.% and (d) 30 wt.% silver. The 25 μm bar applies to all photographs.

Table 1
Silver content calculated and as determined by computerized image analysis

Wt.% silver	Vol.% calculated	Vol.% measured	% silver seen
5	2.18	1.65	76
7.5	3.32	2.44	74
10	4.49	2.96	66
20	957	6.33	66
30	15.36	12.7	83

size. From this information, one can readily calculate the mean silver-to-silver cluster distance. Note that, by mean silver-to-silver distance, is meant the nearest edge-to-edge distance between silver clusters and not the center-to-center distance. This information is summarized in table 2. Note that for the 5 wt.% sample, the mean silver-to-silver distance is on the order of 10 μm, a typical grain size in these materials. As the silver concentration increases, the space available for grains of $Bi_2Sr_2CaCu_2O_8$ to grow is gradually reduced to about half this distance. This provides at least a semi-quantitative understanding as to why the size of the $Bi_2Sr_2CaCu_2O_8$ grains must decrease with increased silver additions: there is simply less room for them to grow. This confirms the qualitative observations made upon examining the photographs; the samples with larger silver additions appear to have a much finer grain structure. That is,

Table 2
Silver clustering characteristics as determined by computerized image analysis

Wt.% silver	Mean cluster density ($N/10^4\ \mu m^2$)	Mean cluster area (μm^2)	Mean silver-to-silver distance (μm)
5	67	2.48	10.4
7.5	93	2.65	8.56
10	96	3.11	8.22
20	151	4.22	5.82
30	114	10.8	5.67

the heavily silver-added samples have many more small grains, and distinctly fewer large ones. Note also that the 30 wt.% sample is somewhat anomalous in that the mean cluster density is lower than that of the 20 wt.% sample. The reason for this, evident in the table under "mean cluster area" and visually apparent in the photographs, is that by 30 wt.% the silver aggregates become very large. It would appear that between 20 and 30 wt.% silver there is a marked increase in the silver cluster size.

These results should be contrasted with $YBa_2Cu_3O_7$ where silver additions, using Ag_2O, have been shown to yield larger grains [11]. The sintering temperatures used for $YBa_2Ca_3O_7$, however, are generally in the range 930°C to 980°C and the atmosphere is usually pure oxygen. Under those conditions, the melting temperature of silver in that matrix can be lower than the sintering temperature. This can result in melt-assisted sintering such that the grains of $YBa_2Ca_3O_7$ grow very large [12]. Also, at the upper end of the $YBa_2Ca_3O_7$ sintering range, the incongruous melting temperature of $YBa_2Ca_3O_7$ in this matrix can be lower than the sintering temperature, which greatly enhances the growth of large $YBa_2Cu_3O_7$ grains [13].

Whenever a known compound is modified chemically as in this work, the question as to whether the silver substitutes into the crystal structure of the $Bi_2Sr_2CaCu_2O_8$ grains is a major issue. Although the optical micrographs discussed above show no silver in the grains, such observations are not very sensitive. In order to look more closely at the $Bi_2Sr_2CaCu_2O_8$ grains themselves, these samples were examined in a scanning electron microscope (SEM) equipped with an energy dispersive X-ray (EDAX) analysis system. The probe beam was focused on individual grains of $Bi_2Sr_2CaCu_2O_8$, away from any obvious silver aggregates. Figure 4 shows typical EDAX results. No silver was seen in any of the grains with this type of analysis. The sample whose spectrum is displayed in the figure is the one with the largest silver concentration, 30 wt.%. The figure shows the characteristic peaks expected for the other constituents, bismuth, strontium, calcium and copper. No silver peaks appear in the spectrum even when the silver region near 3 keV is highly magnified. The lower limit of silver concentration detectable by EDAX is estimated to be 1 to 2 atomic-percent.

Another chemistry issue is the possibility that the presence of silver could alter the relative stoichiometry of the primary constituents of $Bi_2Sr_2CaCu_2O_8$. To check for this possibility, all the samples were subjected to SEM/EDAX analysis in the following way. To the extent possible, the analysis beam was focused on several individual grains of $Bi_2Sr_2CaCu_2O_8$ in each sample. The objective was to determine if samples of varying silver content might show deviations from nominal stoichiometry. The results of this analysis are shown in fig 5. The EDAX intensities have been normalized to copper at 2.0 as indicated by the Cu-labeled arrow to the right of the figure. Each data point represents an average from measurements taken at different locations on a given sample as well as on multiple samples. The error bars on the plot reflect the statistical uncertainty of that averaging. The absolute stoichiometry

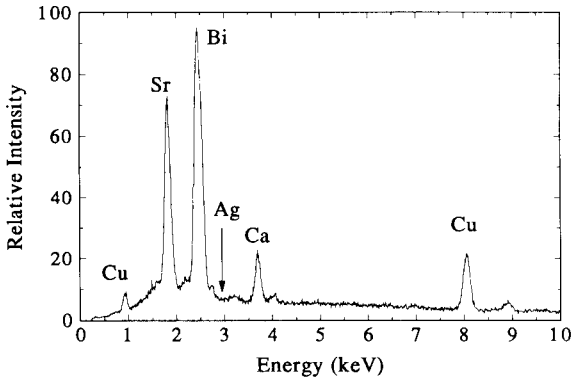

Fig. 4. SEM/EDAX elemental analysis of a typical grain of $Bi_2Sr_2CaCu_2O_8$ in a 30 wt.% silver-added sample; see text.

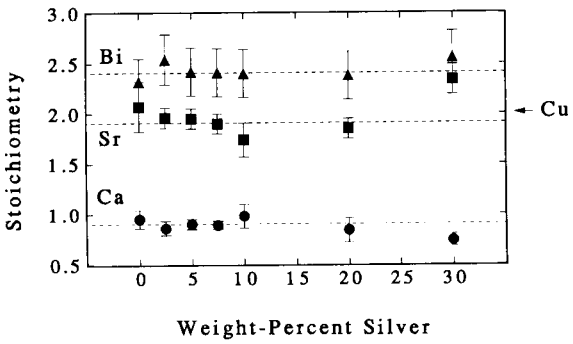

Fig. 5. SEM/EDAX analysis showing the relative stoichiometry of bismuth (triangles), strontium (squares), and calcium (circles) relative to copper as a function of silver content; see text.

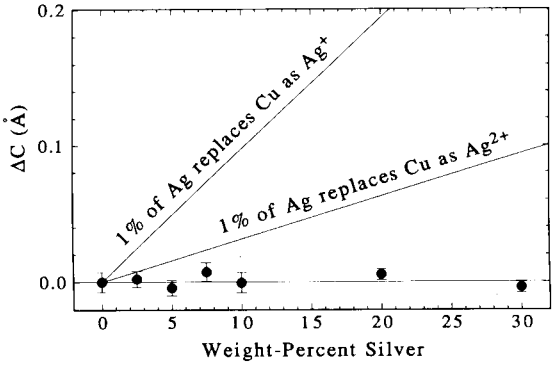

Fig. 6. Measured (circles) and predicted (lines) shift in c-axis spacing of $Bi_2Sr_2CaCu_2O_8$ as a function of silver content; see text.

from such measurements is always in doubt because of matrix effects and the lack of a perfect equivalent standard. In these data, the absolute value for the bismuth stoichiometry is on the high side, whereas the values for calcium and strontium are closer to nominal. The dashed horizontal lines are the average values for the three plotted elements and provide a guide to the eye. Note that there is no significant deviation from the starting stoichiometry as the silver concentration increases. Again, the 30 wt.% sample is somewhat anomalous; it shows a slight reduction in calcium and an increase in strontium.

X-ray diffraction measurements were also performed on these samples. The X-ray peaks of elemental silver are easily seen in all the silver-added samples, as expected. The more interesting question is whether there is any evidence of silver substitution in the $Bi_2Sr_2CaCu_2O_8$ lattice. These measurements were performed using a Rigaku RU-200B X-ray diffractometer. The samples to be X-rayed were pulverized, mixed with an X-ray standard (MoS_2), reground, and sifted through a 45 μm mesh sieve for particle size uniformity. The resulting X-ray spectra were then fit, using approximately 20 major peaks from the previously indexed spectrum of $Bi_2Sr_2CaCu_2O_8$ to determine the lattice parameters. Figure 6 shows the key result of this analysis. The change in c-axis spacing is plotted versus silver content, where $c = 30.80$ Å for the 0 wt.% sample. The error bars are the best estimates of the uncertainty considering both instrumental uncertainty and the statistics of the fit. Also shown are two plausible scenarios in the case that silver might replace copper in the lattice. In both cases, the effect on the c-axis lattice spacing is calculated assuming that 1% of the added silver atoms replace copper atoms [14]. The lower line is computed based on ionic radius of Ag^{2+}; the upper line is for Ag^{+}. We therefore conclude that silver is not going into the lattice to any appreciable extent even in the heavily silver-added samples under the sintering conditions used.

Another issue regarding the the possible effect of silver additions is grain alignment. Grains of $Bi_2Sr_2CaCu_2O_8$ are readily aligned due to the platelet-like morphology of this material. The effect of grain orientation with $Bi_2Sr_2CaCu_2O_8$ is readily seen by X-ray diffraction measurements on powdered samples. Mechanically pressing the powder on the sample mount produces measurable c-axis orientation as compared to loosely sprinkled powder, for example. To obtain some measure of the effect of silver content on orientation, the surfaces of all the pellets were X-rayed. All the samples were pressed in the same die at the same pressure, so one would not expect there to be much sample-to-sample variation. The results of this analysis are shown in fig. 7. Peak height ratios of two different c-axis peaks relative to two non-c-axis peaks are plotted versus silver content. The intensity ratio (0 0 10)/(1 1 5) is the upper plot with the solid line connecting circles; the intensity ratio (0 0 12)/(2 0 0) is the lower plot with the dashed line connecting squares. Although the X-ray beam penetrates to only a shallow depth, it appears that, at least in this surface region, there is a

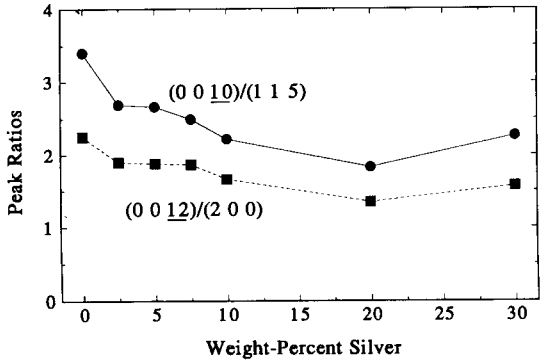

Fig. 7. Ratio of two c-axis peaks to two non-c-axis peaks for $Bi_2Sr_2CaCu_2O_8$ vs. silver content; see text.

reduction in the natural pressed-pellet c-axis alignment with increased silver content. As in several previous instances, the 30 wt.% sample is somewhat anomalous.

The pellets prepared as described above were approximately 22 mm in diameter and 2 mm thick. They were cut into rectangular bars approximately 15 mm long with cross sections of 4 mm^2. Low resistance electrical contacts were made to the samples by baking on silver-paint pads, and then attaching leads to the silver pads with indium solder. The transport critical current density, J_c^{tr}, reported in this paper was measured with a pulsed-DC technique as described in a previous publication [15]. Briefly, a low duty-cycle ($<0.2\%$) pulse is applied to the sample at a low frequency (3.7 Hz), and windows on the voltage and current pulses are repeatedly sampled with a box-car signal averager. The critical current, for a fixed temperature, is then determined by increasing the amplitude of the current pulse until the voltage measured is greater than a specified voltage. For these measurements, an electric field criterion of approximately 2.5 $\mu V/cm$ was used.

The results of such transport critical current measurements on a set of $Bi_2Sr_2CaCu_2O_8$ samples are shown in fig. 8. In the figure, the transport critical current density, J_c^{tr} is shown for samples with no silver (control samples), and with 3, 7.5, 10 and 15 wt.% silver. These measurements were all taken with the samples mounted on a copper sample holder inside a closed-cycle refrigerator. The temperature of the sample was measured with a silicon diode, calibrated to within 0.1 K, attached to the copper sample holder. In addition, a differential thermocouple, connected between the copper sample holder and the grounded current contact on the sample, was used to measure and correct for any temperature difference between the sample holder and sample. This correction was usually no more than a few degrees Kelvin. The actual stabilized temperature at which the measurements were made was slightly different from day to day, averaging (20.7 ± 2.2) K. However, at this temperature the critical current for these samples is not very sensitive to small changes in temperature.

Transport critical current measurements on sintered ceramic superconductors are often plagued by irreproducibility. Microcracking and local variations in porosity can cause different critical currents to be measured on different parts of the same sample, as well as on the same sample on succeeding days due to cracking on handling and due to thermal stress on cooling and warming. Great care was taken with these samples in order to minimize such effects. Instead of the usual 4-probe configuration of contacts, these bar-shaped samples had 5 contacts each. The outer two contacts were always the current leads. Three voltage taps on the inner section of the sample then allowed three different measurements of the critical current by measuring the voltage across

(1) the total (longest) length of the section,

(2) the left portion of the section, and

(3) the right portion of the section. The critical current obtained by sampling the voltage across the total section. J_c^{total}, should agree with the minimum of the other two, J_c^{min}, since the weakest link limits the critical current. Some measure of how the results agree with this assertion can be obtained by looking at the value of $|J_c^{min} - J_c^{total}| / J_c^{min}$. Averaging the results of all the measurements presented here yields a value of (0.019 ± 0.017) for this quantity, showing good consistency on measurements made on different parts of the same sample. Thus, in fig. 8, multiple data points indicate either measurements made on different samples or measurements taken across different voltage taps of the same sample. Because the measured critical current for different parts of the same sample can vary, values near the upper range for each concentration are probably most representative of the true transport critical current. The data indicates that there is a slight increase in the trans-

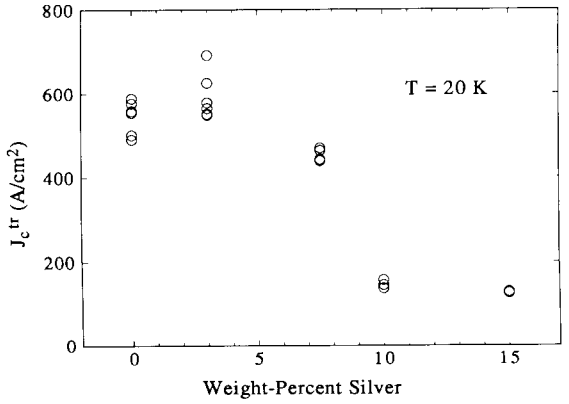

Fig. 8. The transport critical current density, J_c^{tr}, for $Bi_2Sr_2CaCu_2O_8$ with varying silver content; see text.

port critical current for the lower concentrations of silver, followed by a marked decrease in critical current as the silver concentration increases.

Regarding the peak in J_c as a function of silver content (near 3 wt.% silver) seen in fig. 8, it should be pointed out that similar observations have been made with $YBa_2Ca_3O_7$. At least for those reporting increases in J_c in $YBa_2Cu_3O_7$ with silver additions, a peak was always found at rather low silver concentrations; peaks have been reported at 5 [16], 7 [17], and 10 wt.% silver The value of J_c always decreases markedly above these concentrations of silver. Such low concentrations of silver should have very little effect on the percolation path of supercurrent through the material. In the case of $Bi_2Sr_2CaCu_2O_8$, the decrease in J_c is likely due, at least in part, to the increased number of weak links which result from the ever-finer, smaller grain structure in the heavily silver-added samples. Another, more difficult to quantify factor, is the subtle effect of additional components on sintering. That is, when silver, silver oxide, oxygen, lead, or other components are added to the sintering mix, thermodynamic quantities such as melting temperatures, as well as sintering temperatures, change. Based on the references cited in the introduction, it appears that the dominant effect of silver additions to $YBa_2Ca_3O_7$ is a reduction of the melting and optimum sintering temperatures. The situation is less clear for $Bi_2Sr_2CaCu_2O_8$, since the samples are more than 100°C below the melting temperature of silver. However, the process temperature is rather close to the melting temperature of $Bi_2Sr_2CaCu_2O_8$. The sintered quality of these samples is known to change dramatically near the melting temperature. A lowering of the $Bi_2Sr_2CaCu_2O_8$ melting temperature with increased silver additions would mean that the heavily silver-added samples are being sintered closer to their melting temperatures. In other words, at the (constant) sintering temperature used for all samples, the heavily silver-added samples may be more thoroughly sintered. Slight differences in the sintering conditions, due to the addition of silver, could also explain the modest increase in transport J_c observed for low silver concentrations.

The transport critical current density, though very important for most practical applications, is just one measure of the current carrying capacity of granular superconductors. The transport critical current density for sintered samples is usually a measure of the weak links between grains, and as such is often a function of the processing conditions [19], rather than being an intrinsic property of the material. Equally important is the intrinsic intragranular critical current – the maximum current carried by the individual grains. This can be considered some measure of the maximum transport current that could be carried in ideally processed samples, that is, samples with no weak links. For this paper, the intragranular critical current density, referred to here as the magnetization critical current density, J_c^m, was inferred from magnetic hysteresis loops according to Bean's model [20].

The results of such magnetic measurements made on a subset of the $Bi_2Sr_2CaCu_2O_8$ samples with data shown in fig. 8, is illustrated in fig. 9. These data were taken with a SQUID magnetometer, programmed to subject all the samples to the same magnetic history. The samples were cooled in zero magnetic field to the measurement temperature. The magnetic field was then incrementally increased to 20 kG, and finally decreased back to zero. On this slow magnetic loop, the system temperature and field were stabilized, and the magnetic moment measured at fields of 0.01, 1, 5, 10, 20, 10, 5, 1 and 0.01 kG. As indicated in the figure, these data were taken at a temperature of 6 K. The intragranular critical currents inferred were almost 10^6 A/cm^2. This number comes from the measured magnetization difference be-

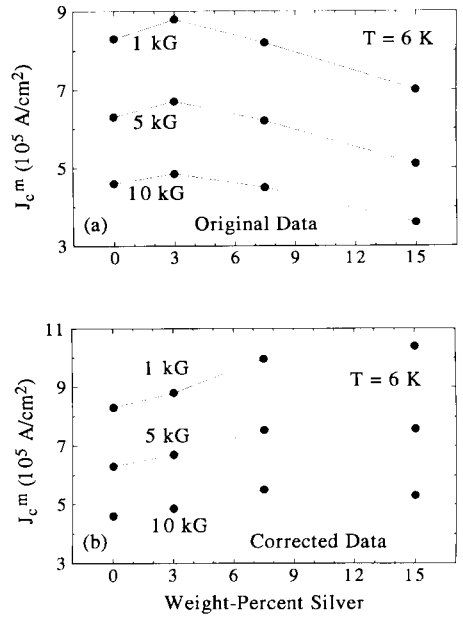

Fig. 9. Magnetization critical current, J_c^m, vs. silver content for $Bi_2Sr_2CaCu_2O_8$; (a) original uncorrected data, and (b) data corrected for grain size effects due to silver; see text.

tween the upper and lower branches of the magnetic hysteresis loop at the respective magnetic field. The difference between the two parts of the figure is that in part (a) no correction is made for the change in grain size with added silver, whereas in part (b) a first order correction to the change in grain size with added silver is made. The morphology of these materials is very complicated as is evident by a microscopic examination of the samples. It is virtually impossible with such sintered samples to arrive at a precise measure of the grain size on even an average basis. The approximate correction made in part (b) of the figure comes from the computerized image analysis; in particular, it comes from the results shown in table 2. As shown in table 2, the mean silver-to-silver distance at 5 wt.% silver is approximately 10 μm, a reasonable value for the mean grain size without silver additions. A grain size of 10 μm was used to compute all the values of J_c^m in part (a) of fig. 9. As the silver concentration increases, the space available for $Bi_2Sr_2CaCu_2O_8$ grains to grow is gradually reduced to approximately 6 μm at 30 wt.% silver. This mean silver-to-silver distance is a rough measure of the maximum size the grains can be and this distance, column 4 of table 2 in particular, was used as a first order correction to the grain size. Making this adjustment to the magnetization loop data in the Bean's model estimate of the intragranular critical current density yields part (b) of the figure.

Using magnetization data to determine the intragranular critical current density introduces a very large uncertainty because of the direct dependence of the deduced J_c on grain size, a number very difficult to determine with any precision in sintered materials. The problem is further complicated because the sintering conditions, which affect the grain size, change in subtle ways due to the silver additions. The raw unadjusted data of fig. 9(a) shows a slight reduction in intragranular critical current, while applying a plausible correction to the grain size shows a slight increase, as shown in fig. 9(b). Given the uncertainty inherent in quantitatively determining changes in grain size, these data cannot be used to argue convincingly that silver additions have any enhancing effect on the intrinsic critical current density of $Bi_2Sr_2CaCu_2O_8$.

4. Summary

Up to 30 wt.% silver, in the form of silver peroxide, has been added prior to the final sintering step in the preparation of $Bi_2Sr_2CaCu_2O_8$. The final sintering step with silver present was performed at 848°C for 20 h in air. Under these conditions, no evidence is found either for the inclusion of silver in the $Bi_2Sr_2CaCu_2O_8$ lattice, or of any adverse chemical reactions that might affect the stoichiometry due to the silver additions. However, the presence of silver does affect sample morphology in several ways. Silver additions interfere with the grain growth resulting in smaller grains of $Bi_2Sr_2CaCu_2O_8$ with increasing concentrations of silver. The intergranular, weak-link critical current density increases for silver additions up to approximately 3 wt.%. For higher concentrations of silver, the intergranular critical current density decreases presumably because the finer grain structure of the highly silver-added samples results in more weak links. The intragranular, intrinsic critical current density also increases as the silver concentration is increased from 0 to 3 wt.%.

For higher silver concentrations, the intragranular critical current density appears to decrease (the magnetization loops decrease in size) if one does not take into account the effect of the silver on the $Bi_2Sr_2CaCu_2O_8$ grain size. However, when the results of a computerized image analysis of the silver-added samples are used as a first-order correction to the grain size, the intragranular critical current density shows only a modest but monotonic increase in the intragranular critical current density with increased silver additions (up to the highest silver concentrations used for these measurements, 15 wt.%). Given the very approximate nature of the grain size correction, this observation is consistent with the conclusion, based on EDAX and X-ray diffraction measurements, that silver does not substitutionally enter the $Bi_2Sr_2CaCu_2O_8$ crystal structure.

Acknowledgements

The authors acknowledge the Independent Research (IR) program at the RDT&E Division of the Naval Command, Control and Ocean Surveillance Center (NCCOSC) for supporting this research and for establishing the research program in high-T_c superconductivity at NCCOSC. The Office of Naval Technology (ONT), through the Wide Area Undersea Surveillance Block Program, and the Strategic Defense Initiative Office (SDIO) are also acknowledged for support of the high-current and high-power conductor development effort at NCCOSC of which this work was a part.

References

[1] Juh Tzeng Lue, J.H. Kung, H.H. Yen, Y.C. Chen and P.T. Wu, Mod. Phys. Lett. B 2 (1988) 589.
[2] P.N. Peters, R.C. Sisk, E.W. Urban, C.Y. Huang and M.K. Wu, Appl. Phys. Lett. 52 (1988) 2066.
[3] B. Dwir, M. Affronte and D. Pavuna, Physica C 162–164 (1989) 351.
[4] T.H. Tiefel, S. Jin, R.C. Sherwood, M.E. Davis, G.W. Kammlott, P.K. Gallagher, D.W. Johnson Jr., R.A. Fastnach and W.W. Rhodes, Mater. Lett. 7 (1989) 363.
[5] Vladimir Plechacek, Vaclav Landa, Zdenek Blazek, Jiri Sneidr, Zanna Trejbalova and Miroslav Cermak, Physica C 153–155 (1988) 878.
[6] S.X. Dou, K.H. Song, H.K. Liu, C.C. Sorrell, M.H. Apperley, A.J. Gouch, N. Savvides and D.W. Hensley, Physica C 160 (1989) 533.
[7] S.X. Dou, K.H. Song, H.K. Liu, C.C. Sorrell, M.H. Apperley and N. Savvides, Appl. Phys. Lett. 56 (1990) 493.
[8] K. Heine, J. Tenbrink and M. Thöner, Appl. Phys. Lett. 55 (1989) 2441.
[9] W.C. McGinnis, T.E. Jones, E.W. Jacobs, P.M. Thibado, R.D. Boss and S. Oseroff, Bull. Amer. Phys. Soc. 35 (1990) 294;
also, T.E. Jones, W.C. McGinnis and J.S. Briggs, Bull. Amer. Phys. Soc. 37 (1992) 334.
[10] T.E. Jones, J.W. Schindler, R.D. Boss, P.M. Thibado and W.C. McGinnis, Phys. Rev. B 41 (1990) 7197.
[11] T.H. Tiefel et al., op. cit.
[12] ibid.
[13] ibid.
[14] James E. Huheey, Inorganic Chemistry, 2d ed. (New York, Harper & Row 1978) p. 71.
[15] W.C. McGinnis, E.W. Jacobs, C.D. Rees and T.E. Jones, Rev. Sci. Instrum. 61 (1990) 984.
[16] Juh Tzeng Lue et al., op. cit.
[17] Mineo Itoh, Hiroyuki Ishigaki, Takashi Ohyama, Takumi Monemoto, Hiroyuki Nojiri and Mitsuhiro Motokawa, J. Mater. Res. 6 (1991) 2272.
[18] B. Dwir et al., op. cit.
[19] W.C. McGinnis, T.E. Jones, E.W. Jacobs, R.D. Boss and J.W. Schindler, IEEE Trans. Magn. 25 (1989) 2138.
[20] C.P. Bean, Phys. Rev. Lett. 8 (1962) 250.